JOC Article

Multifunctional Ferrocene−Ruthenocene Dyads Linked by Single or Double Aza-Containing Bridges Displaying Metal−Metal Interactions and Cation Recognition Properties

Antonio Caballero, Rafaela García, Arturo Espinosa, Alberto Tárraga,* and Pedro Molina*

Departamento de Química Orgánica, Facultad de Química, Universidad de Murcia, Campus de Espinardo, E-30100 Murcia, Spain

pmolina@um.es; atarraga@um.es

Received September 13, 2006

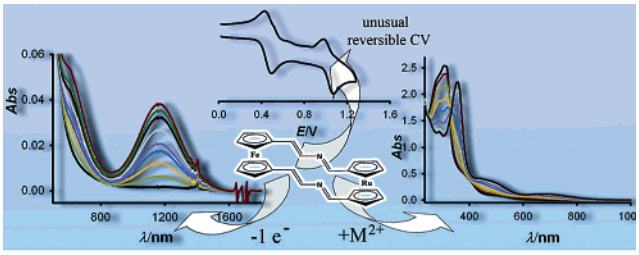

The synthesis, electrochemical, electronic, and cation sensing properties of the ruthenocene-terminated 2-aza-1,3-butadiene **2**, linear ferrocene−ruthenocene dyads **3** and **5**, and the new structural motifs diaza-[4.4]ruthenocenophane **7** and mixed ferrocene and ruthenocene metallocenophanes **8** and **10** are presented. The properties of these compounds have been systematically varied by introducing the ferrocene and ruthenocene moieties at the 1- or 4-position of the unsymmetrical 2-aza-1,3-butadiene bridge. Spectroelectrochemical studies of compounds **3** and **8**, in which the ruthenocene unit appended at the 1-position of the bridge exhibits a rather unusual electrochemical behavior, revealed the presence of low-energy bands in the near-infrared (NIR) region in the partially oxidized forms, at 1070 and 1163 nm, respectively, which indicate the existence of intramolecular charge transfer between the iron and the ruthenium centers. The electrochemical and intermetallic charge-transfer (MMCT) studies (H_{AB}, λ and α parameters) indicate that the $\mathbf{3}^{\bullet+}$ and $\mathbf{8}^{\bullet+}$ systems belong to the Class II classification for a mixed-valence compound. In addition, the low-energy (LE) band of the absorption spectra of all compounds prepared, except compound **10**, are red-shifted by complexation with divalent Mg^{2+}, Zn^{2+}, Cd^{2+}, Hg^{2+}, and Ni^{2+} metal ions. For open dyads, biruthenocene compound **2** exhibited the higher red-shift by 92 nm, whereas for closed compounds the [4.4]ruthenocenoferrocenophane **8** displayed a remarkable red-shift by about 180 nm for Zn^{2+}, Cd^{2+}, Hg^{2+}, and Ni^{2+} metal ions and by about 146 nm for Mg^{2+} cation. The changes in the absorption spectra are accompanied by dramatic color changes which allow the potential for "naked eye" detection. The experimental data and conclusions are supported by DFT computations.

Introduction

Bishomometallocenes assembled on π-conjugated framework have received immense interest in recent years with respect to their electrochemical, electronic, and magnetic properties. The use of redox active polymetallic complexes linked by a π-electron-conjugated systems offers fascinating perspectives for those interested in molecular-level electronics.[1]

Ferrocene systems have been attractive candidates for studying mixed-valence behavior,[2] since ferrocene has a well-developed organic chemistry, allowing attachment to a wide variety of bridges, high stability in both the oxidized and neutral states, and charge-transport ability. Many studies on linked bis-(ferrocenyl) compounds have been reported and have been comprehensively reviewed.[3]

Bis(ruthenocenyl) compounds have been much less studied, presumably partly because of the irreversible redox chemistry of ruthenocene itself. Recently, however, it has been found that diruthenocene, 1,2-bis(ruthenocenyl)ethenes, ruthenocene-terminated butadienes and hexatrienes, and 1,2-bis(ruthenocenyl)-ethynes undergo chemically (though not electrochemically) reversible two-electron oxidations in which a remarkable

10.1021/jo0618932 CCC: $37.00
Published on Web 01/17/2007

structural rearrangement to give η^6-fulvene dications was observed.[4] These formally ligand-based oxidations can be contrasted to the metal-based oxidations of iron analogues; presumably, the small differences in energy between the highest π-orbital and the ruthenium d-orbitals are important, along with the greater tendency of ruthenium to adopt η^6-coordination and to retain an 18 electron configuration. In this respect, ruthenocene resembles an organic fragment more than ferrocene does. Bimetallocenes complexes containing two different types of metal are generally less straightforward to prepare than symmetrical species. This appears to be the reason why they have been studied only in a few cases[5] and why only one example of conjugated ferrocene−ruthenocene derivative has been recently reported.[6]

On the basis of these works, we have designed "open" and "closed" dyads containing both ferrocene and ruthenocene units as redox centers, linked through aza-conjugated bridges which additionally comprise a putative cation-binding site. These molecular systems would exhibit richer electronic interactions and multiple redox properties because electronic communication would occur between iron and ruthenium redox centers, respectively. Furthermore, the electronic effect mediated by the asymmetric bridging ligand is likely tunable by modifying the relative position of the metallocenes in the bridge. On the other hand, the nitrogen atom present in the aza-bridge of this kind of molecules adds another interesting and useful function such as its ability to act as metal-ion ligand.[7] Consequently, the preparation of ferrocene−ruthenocene dyads, with aza-substituted bridges, could be of interest for the construction of heterobimetallic systems which can behave not only as suitable models to study the intramolecular charge transfer across aza-conjugated linkers but also as redox-switching receptors, with the capability of selectively sensing metal-ion guests.[8]

Results and Discussion

Synthesis. Condensation of diethyl aminomethylphosphonate[9] with 1-formylruthenocene[10] provides the N-substituted diethyl aminomethylphosphonates **1**, in almost quantitative yields. Generation of metalloylide, by reaction with *n*-BuLi at −78 °C, and subsequent reaction with the appropriate 1-formylmetallocene provided the 1,4-dimetallocenyl-2-aza-1,3-butadienes **2** and **3** in excellent yields (80−85%). Likewise, starting from the N-substituted diethyl aminomethylphosphonate ferrocene derivative[11] **4** and using 1-formylruthenocene, dyad **5** was obtained in 78% yield. The new structural motifs diaza[4.4]-ruhenocenophane **7** and bimetallocenophanes **8** and **10** were prepared using the same methodology and 1,1′-diformylmetallocenes as building blocks. Thus, condensation of 1,1′diformylruthenocene[10] with diethyl aminomethylphosphonate afforded the corresponding bis(aminomethylphosphonate) ruthenocene derivative **6** which, by metalation followed by reaction with the appropriate 1,1′-diformylmetallocene, led to the homobimetallic metallocenophane **7** and heterobimetallic metallocenophane **8** in 40% and 32% yield, respectively. The isomeric heterobimetallic metallocenophane **10** was prepared in 25% yield from the bis(aminomethylphosphonate) ferrocene derivative[7b] **9** and 1,1′-diformylruthenocene, following the same protocol (Scheme 1).

The ruthenocene-terminated 2-aza-1,3-butadiene **2**, linear heterobimetallocenes **3** and **5**, diaza[4.4]ruthenocenophane **7**, and bimetallocenophanes **8** and **10** were fully characterized using ^{1}H and ^{13}C NMR and EI or FAB mass spectrometry. The analysis of their ^{1}H NMR spectra revealed the following facts: (1) appearance of four pseudotriplets assigned to the eight protons of the two monosubstituted Cp rings; (2) the signals corresponding to those protons in the ruthenocene moiety are deshielding with repect to those located within the ferrocene subunit; and (3) the presence of one singlet and two doublets, corresponding to the protons present in the 2-aza-1,3-butadiene bridge. Assigment of the configuration of the double bonds present in the 1,4-dimetallocenyl-2-aza-1,3-butadienes was achieved by inspection of the corresponding ^{1}H NMR spectroscopic data. The E-configuration of the carbon−carbon double bond, as is expected in a Horner−Wadsworth−Emmons olefination process, was confirmed by the value of the vicinal coupling constants (J = 13.0 Hz). In addition, NOE and two-dimensional NOESY experiments carried out on $CDCl_3$ solutions confirmed the (E,E)-configuration of the double bonds present in the bridge.[11]

Optical and Electrochemical Properties. The UV/vis spectrum of 1,4-bis(ruthenocenyl)-2-aza-1,3-butadiene **2** is characterized by an intense ligand-centered absorption band at

(1) (a) Astruc, D. *Acc. Chem. Rev.* **1997**, *30*, 383. (b) Joachim, C.; Gimzewski, J. K.; Aviram, A. *Nature* **2000**, *408*, 541. (c) Segal, D.; Nitzan, A.; Davis, W. B.; Wasielewski, M. R.; Ratner, M. A. *J. Phys. Chem. B* **2000**, *104*, 3817. (d) Paddow-Row, M. N. In *Electron Transfer in Chemistry*; Balzani, V., Ed.; Wiley-VCH: Weinheim, Germany, 2001; Vol. 2, p 179. (e) De Cola, L.; Belser, P. In *Electron Transfer in Chemistry*; Balzani, V., Ed.; Wiley-VCH: Weinheim, Germany, 2001; Vol. 5, p 97. (f) Kilsa, K.; Kajanus, J.; Macpherson, A. N.; Martensson, J.; Albinsson, B. *J. Am. Chem. Soc.* **2001**, *123*, 3069. (g) Launay, J.-P. *Chem. Soc. Rev.* **2001**, *30*, 386. (h) Newton, M. D. *Chem. Rev.* **1991**, *91*, 767. (i) Nelsen, S. F.; Ismagilov, R. F.; Powell, D. F. *J. Am. Chem. Soc.* **1998**, *120*, 1924. (j) Davis, D. F.; Svec, W. A.; Ratner, M. A.; Wasielewski, M. R. *Nature* **1998**, *396*, 60. (k) Ceccon, V.; Santi, V.; Orian, L.; Bisello, A. *Coord. Chem. Rev.* **2004**, *248*, 683.

(2) Hush, N. S. *Coord. Chem. Rev.* **1985**, *64*, 135.

(3) Barlow, S.; O'Hare, D. *Chem. Rev.* **1997**, *97*, 637.

(4) (a) Sato, V.; Kudo, A.; Kawata, Y.; Saitoh, H. *Chem. Commun*. **1996**, 25. (b) Sato, M.; Kawata, Y.; Kudo, A.; Iwai, A.; Daitoh, H.; Ochiai, S. *J. Chem. Soc., Dalton Trans*. **1998**, 2215. (c) Watanabe, M.; Sato, M.; Takayama, T. *Organometallics* **1999**, *18*, 5201. (d) Sato, M.; Maruyama, G.; Tanemura, A. *J. Organomet. Chem.* **2002**, *655*, 23. (e) Sato, M.; Watanabe, M. *Chem. Commun*. **2002**, 1574. (f) Sato, M.; Suzuki, M.; Okoshi, M.; Kurasina, M.; Watanabe, M. *J. Organomet. Chem.* **2002**, *648*, 72. (g) Sato, M.; Nagata, T.; Tanemura, A.; Fujihara, T.; Kamakura, S.; Unoura, K. *Chem. Eur. J.* **2004**, *10*, 2166. (h) Sato, M.; Kubota, Y.; Kawata, Y.; Fujihara, T.; Unoura, Kei.; Oyama, A. *Chem. Eur. J.* **2006**, *12*, 2282.

(5) (a) Watanabe, M.; Motoyama, I.; Takayama, T. *J. Organomet. Chem.* **1996**, *524*, 9. (b) Neuse, E. W.; Loonat, M. S. *Transition Met. Chem.* **1981**, *260*, 6. (c) Watanabe, M.; Sano, H. *Chem. Lett.* **1989**, 1345. (d) Watanabe, M.; Sano, H. *Bull. Chem. Soc. Jpn.* **1990**, *63*, 777. (e) Watanabe, M.; Masuda, Y.; Motoyama, I.; Sano, H. *Bull. Chem. Soc. Jpn.* **1988**, *61*, 827. (f) Watanabe, M.; Motoyama, I.; Takayama, T. *Bull. Soc. Chim. Jpn.* **1996**, *69*, 2877.

(6) Obendorf, D.; Schottenberger, H.; Wurst, K.; Schuler, N.; Laus, G. *J. Organomet. Chem.* **2005**, *690*, 811.

(7) (a) Caballero, A.; Tormos, R.; Espinosa, A.; Velasco, M. D.; Tárraga, A.; Miranda, M. A.; Molina, P. *Org. Lett.* **2004**, *6*, 4599. (b) Caballero, A.; Lloveras, V.; Tárraga, A.; Espinosa, A.; Velasco, M. D.; Vidal-Gancedo, J.; Rovira, C.; Wurst, K.; Molina, P.; Veciana, J. *Angew. Chem., Int. Ed.* **2005**, *44*, 1977. (c) Caballero, A.; Tárraga, A.; Velasco, M. D.; Espinosa, A.; Molina, P. *Org. Lett.* **2005**, *7*, 3171.

(8) (a) Constable, E. C. *Angew. Chem., Int. Ed. Engl.* **1991**, *30*, 407. (b) Beer, P. D. *Adv. Inorg. Chem.* **1992**, *39*, 79.

(9) Davidsen, S. K.; Phillips, G. W.; Martin, S. F. *Org. Synth.* **1983**, *8*, 451.

(10) 1-Formylruthenocene and 1,1′-diformylferrocene were prepared by mono- and dilithiation of ruthenocene and subsequent reaction with DMF, following a modification of the previously described procedure: Sanders, R.; Mueller-Westerhoff, U. T. *J. Organomet. Chem.* **1996**, *512*, 21.

(11) Lloveras, V.; Caballero, A.; Tárraga, A.; Velasco, M. D.; Espinosa, A.; Wurts, K.; Evans, D. J.; Vidal-Gancedo, J.; Rovira, C.; Molina, P.; Veciana, J. *Eur. J. Inorg. Chem*. **2005**, 2436.

SCHEME 1. Synthesis of Compounds 2, 3, 5, 7, 8, and 10[a]

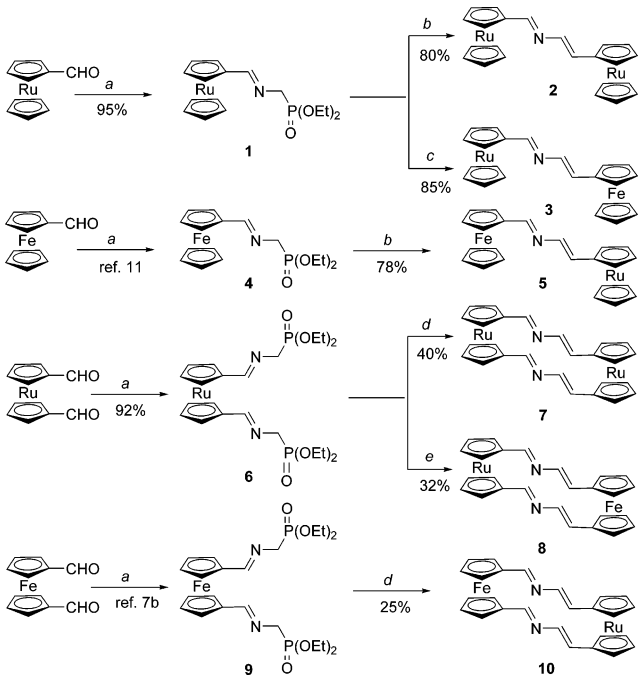

[a] Reagents. (*a*) (i) Diethylaminomethylphosphonate/CH_2Cl_2/rt (ii) anhydrous Na_2SO_4; (*b*) (i) *n*-BuLi/−78 °C (ii) 1-formylruthenocene; (*c*) (i) *n*-BuLi/−78 °C (ii) 1-formylferrocene; (*d*) (i) *n*-BuLi/−78 °C (ii) 1,1′-diformylruthenocene; (*e*) (i) *n*-BuLi/−78 °C (ii) 1,1′-diformylferrocene.

313 nm along with a low-energy absorption band at 365 nm, which is ascribed to a Ru^{II}-to-ligand (MLCT) transition.[12] The spectra of heterobimetallocenes **3** and **5** could be explained on the basis of the individual ferrocene and ruthenocene components of each dyad. Thus, in addition to the low-energy band due to the ruthenocene moiety, another weaker low-energy absorption band is visible between 448 and 464 nm, which is produced either by nearly degenerate transitions, a Fe^{II} d−d transition,[12] or a Fe^{II}-to-ligand LMCT process ($d_\pi-\pi_*$).[13] Similar UV/vis spectra exhibit the [4.4]ruthenocenophane **7** and bimetallocenophanes **8** and **10**, in which the low-energy absorption band is red-shited by 44 nm, for compound **8,** and 15 nm, for compound **10** (Table 1).

Electrochemical studies, carried out in a CH_3CN/CH_2Cl_2 (3/2, v/v) solution, revealed that dyads **2**, **3**, and **5** show electroactivity because of the presence of both metallocene units. The relative oxidation potentials of the redox processes were determined by both cyclic (CV) and differential pulse (DPV) techniques. The CV of dyad **2** clearly showed an irreversible electrochemical behavior ($\Delta E = E_{pc} - E_{pa} = 0.18$ V), and the oxidation wave was accompanied by a reduction wave with nearly the same magnitude as that of the oxidation wave ($i_{pa}/i_{pc} = 1.2$). The electron count (*n*), obtained from coulometry, is nearly 2.0, providing that the observed wave corresponds to a two-electron process. In the CV of **5**, two irreversible oxidative processes were observed at approximately 0.68 and 0.90 V,

TABLE 1. Table UV−Vis/Near-IR Data in CH_2Cl_2

compd	λ_{max}[nm] (10^{-3} ϵ[$M^{-1}cm^{-1}$])
2	313 (10.72), 365 (7.31)
2$^{2+\,a}$	**353 (3.21), 447 (2.04)**
3	322 (18.22), 364 (sh), 448 (1.75)
3$^{\bullet+\,a}$	322 (9.83), 364 (sh), 416 (5.22), 518 (2.74), 1070[b] (0.25)
3$^{2+\,a}$	**349 (7.74), 435 (5.65), 903 (0.48)**
5	331 (10.21), 362 (sh), 464 (1.27)
5$^{\bullet+\,a}$	331 (6.44), 362 (sh), 446 (sh), 531 (1.41), 1246[b] (0.027)
5$^{2+\,a}$	**356 (2.96), 531 (1.33), 971 (0.046)**
7	297 (20.72), 334 (sh) 395 (sh)
7$^{2+\,a}$	**312 (sh), 321 (20.72), 384 (sh), 480 (sh)**
8	283 (sh), 315 (25.27), 377 (sh), 492 (9.32)
8$^{+\,a}$	290 (17.43), 320 (18.47), 437 (sh), 605 (6.32), 1163[b] (0.44)
8$^{2+\,a}$	**284 (sh), 350 (13.65), 442 (sh), 672 (5.8)**
10	307 (8.41), 317 (8.39), 369 (sh), 479 (1.06)
10$^{2+\,a}$	345 (5.51), 448 (2.17), 547 (1.06)

[a] Oxidized species obtained electrochemically in CH_2Cl_2 (10^{-3} M) using [*n*-Bu_4N][PF_6] (0.15 M) as supporting electrolyte. [b] Values obtained by deconvolution of the experimental spectra.

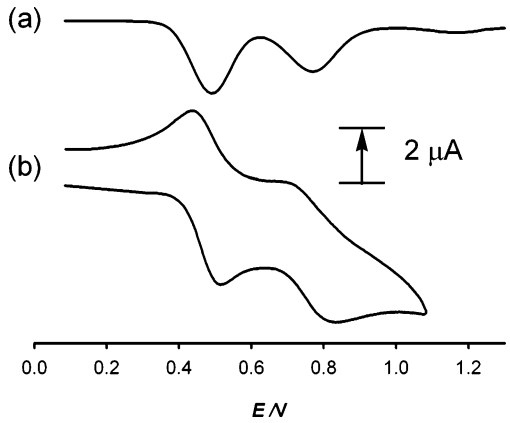

FIGURE 1. Voltammogram of compound **3** (1 mM) in CH_3CN/CH_2Cl_2 (3/2, v/v) using [(*n*-Bu)$_4$N]PF_6 (0.1 M) as supporting electrolyte scanned at 100 mV s^{-1}: (a) DPV from 0.0 to 1.25 V; (b) CV from 0.0 to 1.1 V.

respectively, versus decamethylferrocene (DMFc), and a complex re-reductive process appeared on the turn of the scan at 1.1 V. The nonreversible features in the CVs of **2** and **5** may suggest that the oxidation and reduction peaks represent an electron-transfer process followed by a chemical reaction. Consequently, this irreversible behavior excludes their capability to act as electrochemical switches. Only dyad **3** shows reversible ferrocene/ferricinium redox cycles over time,[14] indicating that it would be suitable for use as an electrochemical sensor. The first reversible oxidation process at 0.51 V versus DMFc (ΔEp = 0.06 V) arises from the one-electron oxidation of the ferrocene unit. The second feature of the CV is associated with a rather unusual quasireversible (ΔEp = 0.11 V) oxidation principally of the ruthenocene unit. Likewise, the DPV voltammogram also exhibits two well-resolved oxidation peaks at formal potentials of +0.51 and +0.80 V versus DMFc (Figure 1). The stability of the mixed valence species **3**$^{\bullet+}$ can be initially estimated from the equilibrium constant (K_c) for the comproportionation process[3] (**3**) + (**3**)$^{2+}$ ⇌ 2 (**3**)$^{+}$ which is evaluated from the electrochemical potential data as $K_c = 8.0 \times 10^4$.

(12) (a) Sohn, Y. S.; Hendrickson, D. N.; Gray, M. B. *J. Am. Chem. Soc.* **1971**, *93*, 3603. (b) Sanderson, C. T.; Quinian, J. A.; Conover, R. C.; Johnson, M. K.; Murphy, M.; Dluhy, R. A.; Kuntal, C. *Inorg. Chem.* **2005**, *44*, 3283. (c) Gao, L.-B.; Zhang, L.-Y.; Shi, L.-X.; Cheng, Z.-N. *Organometallics* **2005**, *24*, 1678.

(13) Barlow, S.; Bunting, H. E.; Ringham, C.; Green, J. C.; Bublitz, G. U.; Boxer, S. G.; Perry, J. W.; Marder, S. R. *J. Am. Chem. Soc.* **1999**, *121*, 3715.

(14) The criteria applied for reversibility was (1) separation of 60 mV between cathodic and anodic peaks, (2) close-to-unity ratio of the intensities of the cathodic and anodic currents I_c/I_a, and (3) constancy of the half-wave potential on changing sweep rate in the CVs. The same half-wave potential values have been obtained from the DPV peaks and from an average of the cathodic and anodic cyclic voltammetric peak.

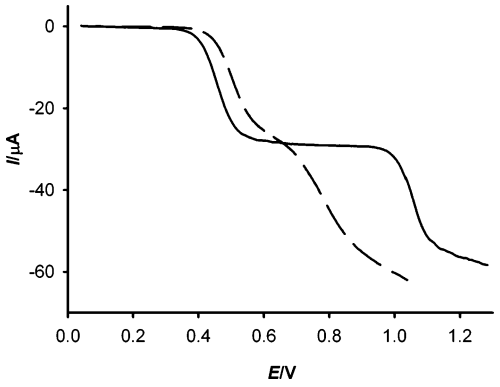

FIGURE 2. Linear sweep voltammogram for compound **3** (dash line) and **8** (solid line), (1 mM) in CH_3CN/CH_2Cl_2 (3/2, v/v) obtained using rotating disk electrode at 100 mV s^{-1} and 1000 rpm.

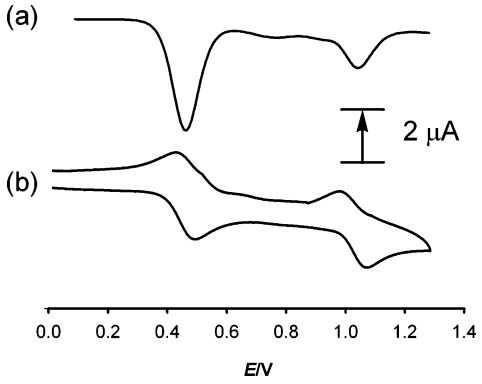

FIGURE 3. Voltammogram of compound **8** (1 mM) in CH_3CN/CH_2Cl_2 (3/2, v/v) using $[(n\text{-}Bu)_4N]PF_6$ (0.1 M) as supporting electrolyte scanned at 100 mV s^{-1}: (a) DPV from 0.0 to 1.20 V; (b) CV from 0.0 to 1.20 V.

A rotating-disk voltammetry experiment has confirmed that the ruthenocene oxidation involves a one-electron process, as evaluated from the comparison of the heights of the Fe^{II}/Fe^{III} and Ru^{II}/Ru^{III} oxidation waves (Figure 2). This assumption is also confirmed by controlled potential coulometry at 1.2 V.

The electrochemical behavior of the ruthenocenophane **7** and bimetallocenophanes **8** and **10** is almost identical to that of the closely related open bimetallocenes. The CV of the diaza-[4.4]-ruthenocenophane **7** clearly shows that the electron transfer is not reversible ($\Delta E = E_{pc} - E_{pa} = 0.18$ V), whereas the DPV exhibits an oxidation peak at formal potential of +65 V versus DMFc. In the CV of **10**, two irreversible oxidative processes were observed at approximately 0.64 and 0.87 V versus DMFc, respectively, and a complex re-reductive process appeared on the turn of the scan at 1.2 V. The DPV voltammogram also exhibits two oxidation peaks at formal potentials of +0.66 and +0.75 V versus DMFc. However, the new structural motif diaza-[4.4]ruthenocenoferrocenophane[15] **8** shows reversible ferrocene/ferricinium redox cycles over time. The first reversible oxidation process at 0.46 V versus DMFc ($\Delta Ep = 0.06$ V) arises from the one-electron oxidation of the ferrocene unit. The second feature of the CV is associated with an unusual quasireversible ($\Delta Ep = 0.11$V) oxidation principally of the ruthenocene unit. Likewise, the DPV voltammogram also exhibits two well-resolved oxidation peaks at formal potentials of +0.46 and +1.01 V versus DMFc (Figure 3). From this electrochemical data, a comproportionation constant $K_c = 4.18 \times 10^8$ was also calculated.

A rotating-disk voltammetry experiment has also confirmed that the ruthenocene oxidation involves a one-electron process, as evaluated from the comparison of the heights of the Fe^{II}/Fe^{III} and Ru^{II}/Ru^{III} oxidation waves (Figure 2). The difference between the oxidation peaks in the heterometallocenophane **8** ($\Delta E = 0.51$ V) is almost twice as large as the value found in the single-bridged dyad **3** ($\Delta E = 0.29$ V). This result confirms those obtained in the ferrocene series[16] according to which in going from "open biheterometallocene" structures to the "closed biheterometallocenophanes" the differences between the redox potential approximately double. These electrochemical data, however, also reflect that the ferrocene unit in the "open" compound **3** is slightly more difficult to oxidize than the ferrocene unit in the "closed" structure **8** (0.51 V vs 0.46 V). By contrast, the ruthenocene moiety in compound **3** is slightly easier to oxidize than the ruthenocene fragment in **8** (0.80 V vs 1.01 V).

The electrochemical behavior of the ruthenocene unit in dyads **3** and **8** is unexpected, because it is well-known that ruthenocene and its derivatives, as opposed to their ferrocene analogues, usually undergo an irreversible one-step two-electron oxidation process.[17] The reasons given for this behavior are either a rapid dimerization of the ruthenocenium (Cp_2Ru^+) species that is generated followed by disproportionation or the direct disproportionation of (Cp_2Ru^+), in the presence of weakly coordinating ligands. However, a quasi-reversible one-electron oxidation of ruthenocene derivatives has only been observed in molten salts,[18] in noncoordinating solvent using a noncoordinating electrolyte,[19] or by introducing steric hindrance around the metal by completely methylating the Cp rings to form Cp_2^*Ru species.[20]

Spectroelectrochemistry. All ruthenocene compounds, such as dyad **2** and [4.4]ruthenocenophane **7**, which only showed one oxidation step by CV, did not display any near-infrared (NIR) absorption band upon oxidation at 1.2 V. This result indicates that the two ruthenium centers were oxidized at the same potential and, therefore, a mixed-valence complex was not produced. Because of the nonreversible features of the CVs of ferrocene−ruthenocene dyad **5** and [4.4]ferrocenoruthenocenonophane **10**, bearing the ferrocene unit at the 1 position of the bridge, all attempts to promote a controlled oxidation process failed. Then, the full oxidized compounds were only obtained in these cases which, in turn, did not display any NIR absorption band. Isosbestic points were found during the oxidation process (Table 1).

Controlled potential absorption spectra of dyad **3,** in which the ferrocene unit is placed at the 4 position of the bridge, in CH_2Cl_2 are shown in Figure 4. On electrochemical one-electron

(15) We denote compound **8** as diaza[4.4]ruthenocenoferrocenophane because the ruthenocenylene and the ferrocenylene units are linked at 1- and 4-positions, respectively, of the unsymmetrical 2-azabridges. Taking into account the same criteria, the regioisomer **10**, in which both metallocene units are exchanged, is named as diaza[4.4]ferrocenoruthenocenophane.

(16) LeVanda, C.; Bechgaard, K.; Cowan, D. O. *J. Org. Chem.* **1976**, *41*, 2700.

(17) (a) Kuwana, T.; Bublitz, D. E.; Hoh, G. *J. Am. Chem. Soc.* **1960**, *82*, 5811. (b) Gubin, S. P.; Smirnova, L. I.; Denisovich, L. I.; Lubovich, A. A. *J. Organomet. Chem.* **1971**, *30*, 243. (c) Denisovich, L. I.; Zakurin, N. V.; Bazrukova, A. A.; Gubin, S. P. *J. Organomet. Chem.* **1974**, *81*, 207.

(18) Gale, R. J.; Job, R. *Inorg. Chem.* **1981**, *20*, 42.

(19) Hill, M. G.; Lamanna, W. M.; Mann, K. R. *Inorg. Chem.* **1991**, *30*, 4687.

(20) (a) Koelle, U.; Salzer, A. *J. Organomet. Chem.* **1983**, *243*, C27. (b) Koelle, U.; Grub, J. *J. Organomet. Chem.* **1985**, *289*, 133.

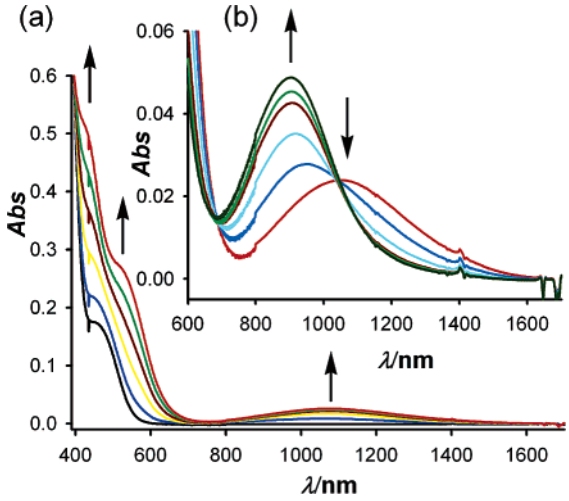

FIGURE 4. Evolution of UV−vis−NIR spectra during the course of the oxidation of compound **3** (1 mM) in CH_2Cl_2 with $[(n\text{-Bu})_4N]PF_6$ (0.15 M) as supporting electrolyte when (a) $0 \le n \le 1$ or (b) $1 \le n \le 2$ electrons are removed. Arrows indicate absorptions that increase or decrease during the experiment.

oxidation, at 0.70 V versus DMFc, the MLTC band at $\lambda_{max} =$ 448 nm ($\epsilon_{max} = 1750$ M^{-1} cm^{-1}) shifted to the red at $\lambda_{max} =$ 518 nm with a decrease in its maximum ($\epsilon_{max} = 2740$ M^{-1} cm^{-1}) as $\mathbf{3}^{+\bullet}$ was formed. Simultaneously, a new band grew in the near-IR region at $\lambda_{max} = 1070$ nm ($\epsilon_{max} = 260$ M^{-1} cm^{-1}), reaching its maximum after complete one-electron oxidation, at 0.70 V. Furthermore, a defined isosbestic point at $\lambda = 395$ nm is maintained during the course of the partial oxidation process. As in the CV, the first redox wave (0.51 V) was assigned to one-electron process occurring at the Fe center ($Fe^{II/III}$); the new absorption band (1070 nm) appearing in the near-IR region after the electrolysis can, therefore, be attributed to the metal−metal charge transfer (MMCT) from the Ru^{II} to Fe^{III} sites (Table 1), as it is discussed in the next section.

Further oxidation at 1.10 V causes the progressive disappearance of the band at 1070 nm and the formation of a new band at higher energy region ($\lambda_{max} = 903$ nm, with $\epsilon_{max} = 490$ M^{-1} cm^{-1}). Interestingly, three well-defined isosbestic points at $\lambda = 395$, 682, and 1040 nm are maintained during the course of this oxidation process (Figure 4). As in the CV, the last oxidation wave (0.80 V) was assigned to the redox process at the Ru site ($Ru^{II/III}$). This newly formed band might be assigned to ligand−Ru^{III} charge transfer (LMCT).[21]

Likewise, generation of the mono-oxidized species derived from the [4.4]ruthenoceneferrocenophane **8**, in which the ferrocene unit is placed at the 4 position of the bridge, was performed by constant potential electrolysis, 0.14 V above $E_{1/2}$ of the ferrocenyl redox couple, and was monitored by absorption spectroscopy. During the oxidation, a new LMCT (Cp−Fe^{III}) band at $\lambda = 605$ nm ($\epsilon = 632$ M^{-1} cm^{-1}) appears with concomitant decreasing of the band at $\lambda = 492$ nm ($\epsilon = 932$ M^{-1} cm^{-1}). Moreover, in the NIR region, a new band at $\lambda =$ 1163 nm ($\epsilon = 443$ M^{-1} cm^{-1}) appears, its intensity continuously increasing until one electron is removed, which is assigned to the metal−metal charge transfer (MMCT) from the Ru^{II} to Fe^{III} sites. Along with the changes of these bands, a defined isosbestic point at $\lambda = 326$ nm is maintained during the course of the

(21) Gao, L-B.; Zhang, L.-Y.; Shi, L.-X.; Chen, Z.-N. *Organometallics* **2005**, *24*, 1678.

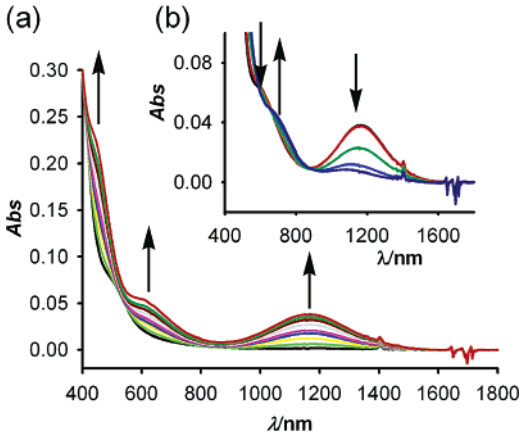

FIGURE 5. Evolution of UV−vis−NIR spectra during the course of the oxidation of compound **8** (1 mM) in CH_2Cl_2 with $[(n\text{-Bu})_4N]PF_6$ (0.15 M) as supporting electrolyte when (a) $0 \le n \le 1$ or (b) $1 \le n \le 2$ electrons are removed. Arrows indicate absorptions that increase or decrease during the experiment.

oxidation process. Interestingly, on removing two electrons, at a constant potential of 1.20 V, the intensity of the band at $\lambda =$ 1163 nm decreases until it disappears when the compound is fully oxidized. At the same time, a new band appears at $\lambda =$ 672 nm ($\epsilon = 580$ M^{-1} cm^{-1}), which could be attributed to a ligand−Ru^{III} charge transfer (LMCT). As in the case of the related "open" compound **3**, three well-defined isosbestic points at $\lambda = 345$, 587, and 653 nm are maintained during the course of this oxidation process (Figure 5).

The application of the two-state Hush[22] model to the spectrum of the mixed-valence compounds $\mathbf{3}^{\bullet+}$ and $\mathbf{8}^{\bullet+}$ predicts a half-height bandwidth [$\Delta\nu_{1/2} = (2310\lambda)^{1/2}$] in the case where the two redox sites are inequivalent[23] of 4039 cm^{-1} and 3015 cm^{-1}, respectively, which were larger than the values determined experimentally (3614 cm^{-1} and 2334 cm^{-1}) by spectral deconvolution assuming a Gaussian profile. The origin of this discrepancy is not immediately clear, although differences between theoretical and experimental values of $\Delta\nu_{1/2}$ are not uncommon. They often arise from system nonidealities with respect to the model.[24] The availability of E_{MMCT} also enables the estimation of the H_{AB} (adiabatic electronic coupling element), which can also be related to the ground-state delocalization coefficient[25] α (Table 2). The λ, the reorganization energy of Marcus theory, and α^2 values are similar to those previously reported for related homonuclear biferrocenes[11] and heteronuclear ferrocene−ruthenium mixed-valence systems.[26]

(22) (a) Hush, N. S. *Prog. Inorg. Chem.* **1967**, *8*, 391. (b) Robin, M. B.; Day, P. *Adv. Inorg. Chem. Radiochem.* **1967**, *10*, 247. (c) Creutz, C. *Prog. Inorg. Chem.* **1983**, *30*, 1. (d) Nelsen, S. F. *Chem. Eur. J.* **2000**, *6*, 581.

(23) Hush theory indicates that for a mixed-valence system with two inequivalent redox centres, the energy of the IVTC transition is given by $\tilde{\nu}_{max} = \lambda + \Delta G_0$, where λ_{max} is the reorganization energy of Marcus theory and ΔG_0 can be estimated from the electrochemical data. If one assumes that the oxidation potential of one center is unaffected by the oxidation state of the other, the magnitud of ΔG_0 is obtained by converting the electrochemical value of $\Delta E_{1/2}$ into energy units. For an elegant application, see: Barlow, S. *Inorg. Chem.* **2001**, *40*, 7047−7053.

(24) (a) Elliot, C. M.; Derr, D. L.; Matyushov, D. V.; Newton, M. D. *J. Am. Chem. Soc.* **1998**, *120*, 11714. (b) Curtis, J. C.; Meyer, T. J. *Inorg. Chem.* **1982**, *21*, 1562.

(25) $H_{AB} = 2.05 \times 10^{-2}$ $(\epsilon_{max}\Delta\tilde{\nu}_{1/2}\tilde{\nu}_{max})^{1/2}/r$ is the Hush equation for the calculation of the electronic interaction in mixed-valence complexes, and $\alpha = H_{AB}/\tilde{\nu}_{max}$ was used to estimate the degree of electronic delocalization.

(26) Dowling, N.; Henry, P. M. *Inorg. Chem.* **1982**, *21*, 4088.

TABLE 2. Parameters Related to the MMCT Bands of Mixed-Valence $3^{\bullet+}$ and $8^{\bullet+}$ Systems

compound[a]	ν_{max} (cm^{-1})	ϵ_{max} (M^{-1} cm^{-1})	λ (cm^{-1})	$\Delta\nu_{1/2exp.}$ (cm^{-1})	$\Delta\nu_{1/2theor}$ (cm^{-1})	d (Å)[b]	H_{AB} (cm^{-1})	α^2
$\mathbf{3}^{\bullet+}$	9346	260	7063	3614	4646	9.344	260[a]	$7.7\cdot10^{-4}$
$\mathbf{8}^{\bullet+}$	8598	443	3936	2334	3015	8.384	230[a]	$7.15\cdot10^{-4}$

[a] MMCT (Fe(II)−Ru(III)). [b] From the calculated structures at B3LYP/6−31G*/Lanl2DZ−ECP level.

Since the Hush model can only be rigorously applied to weakly coupled mixed-valence species, the electrochemical and intermetallic charge-transfer (MMCT) study ($2H_{AB}/\lambda$: 0.073 for $\mathbf{3}^{\bullet+}$ and 0.117 for $\mathbf{8}^{\bullet+}$) indicates that the $\mathbf{3}^{\bullet+}$ and $\mathbf{8}^{\bullet+}$ systems belong to Class II, although observation of a narrower bandwidth than predicted theoretically could suggest that these systems lie close to transition between Class II and II−III classification for a mixed-valence compound.[27] However, the values of the parameter Γ[28] (0.11 for $\mathbf{3}^{\bullet+}$ and 0.23 for $\mathbf{8}^{\bullet+}$) indicate that these mixed-valence compounds are weakly coupled Class II systems.

Theoretical Calculations. Quantum chemical calculations at the DFT level (see Supporting Information) have provided in-depth insight about the different behavior of the studied systems upon oxidation and the occurrence of MMCT (metal−metal charge-transfer) processes. For the sake of comparison, the theoretical study has been extended to the recently reported open-chain 1,4-bis(ferrocenyl)-2-aza-1,3-butadiene **11**[11] and the related closed diaza[4.4]ferrocenophane **12**,[7b] as well as to vinylferrocene **13** and vinyl-ruthenocene **14** as half-system models.

The greater ease of oxidation of ferrocene derivatives in relation to the ruthenocene analogous (oxidation potentials around +0.4 and +1.0 V versus DMFc, respectively) could be analyzed by comparison of the energies and occupancies of the uppermost AO on every metal center, as obtained from the NAO (natural atomic orbital) analysis for model compounds **13** and **14** (see the Supporting Information).

On the other hand, in neutral homobimetallic systems **11** and **2**, the differences between both metallocene units is exclusively due to the polarization of the aza-bridge and therefore Mc_2 (Mc_1 and Mc_2 standing for the metallocene unit at the 1- or 4-position of the bridge, respectively) is expected to be the most electron-rich metallocene moiety, in agreement with the higher negative charge at position C(4) than at C(1) in the parent unsubstituted 2-aza-1,3-butadiene (calculated natural charges −0.341 and −0.019, respectively, at the working level of theory). Consequently, one-electron removal should take place from the metal atom located at that Mc_2 substituent (where Mc_1 is the one closer to the N atom). The above reasoning allows to predict that heterobimetallocenyl derivatives **3** and **5** should undergo initial oxidation at the Fc moiety, this oxidation being easier when the Fc unit is at the C(4) position of the aza-bridge, as in **3**. The same tendency is observed in bimetallocenophanes.

More interesting are the results of the study of electric charge variation along the oxidative sequence at relevant parts of the molecule (Figure 6). For that purpose, every molecular system has been divided in three subunits: two metallocenyl end-caps and the bridge connecting them. For the diaza[4.4]-bimetallocenophanes **7**, **8**, **10**, and **12**, both azadiene linkers are included in the bridge subunit, whereas this subunit corresponds to the vinyl substituent in model compounds **13** and **14**. We have used charges resulting from NBO (natural bond orbital) analysis, although Mulliken charges gave similar results, and have made the assumption that the first one-electron oxidative process can be divided into two steps which can be taken as happening successively and have been named as [*n*]*m*, where the first index between brackets denotes the employed geometry optimized for the system having a net charge "*n*", and the second one refers to the actual charge "*m*" of the system under consideration. Thus, starting from the neutral optimized structures ([0]0), removal of one electron from the highest occupied molecular orbital (HOMO) leads to an unstable radical-cation state ([0]1) with instantaneously redistributed electron density and which thereafter reorganizes its geometry ([1]1) to better accommodate the generated electronic deficiency. Analogously, although not analyzed herein, subsequent removal of a second electron would lead consecutively to dications [1]2 and [2]2.

Several conclusions can be extracted from the inspection of Figure 6. In the neutral form, all azadiene bridges display a small charge (ca. −0.014 or 0.005 au for open or closed systems, respectively), with Mc_1 having more positive charge (range 0.031−0.057 au) than Mc_2 (range −0.033 to −0.008 au) thus indicating the tendency of the azadiene bridge to push electron density in the C(1)→C(4) sense (Figure 6a and b). The reference vinyl-metallocenes **13** and **14** show the expected oxidative response with most of the acquired positive charge (ca. 0.9 au) allocated in the metallocene framework, although a significative difference is observed for **14** where the spin density is partially spread on the vinyl substituent (Figure 6c) suggesting a formal oxidation of the "bridge" (see below).

The above electronic changes upon oxidation are better understood in terms of the geometrical reorganization undergone by every molecular system which, in turn, can be mainly characterized by proper geometrical distortion parameters at the metallocene units (see the Supporting Information). Within the same level of theory, in the ferrocene series the Fe···Cp# distances (where Cp# stands for the Cp ring centroid) are only slightly sensitive to the nature of electron donating or withdrawing groups at the opposite Cp ring (cf. calculated distances $d_{Fe-Cpb\#}$ = 1.675, 1.678, 1.676, 1.676, and 1.677 Å when substituents are −H, $-NH_2$, −OH, $-NO_2$, and −CHO, respectively) but are considerably increased in radical-cation ferricinium species probably because of the removal of an electron slightly bonding with respect to iron-ring interactions, in agreement with both theoretical (calculated Fe···Cp# distance for the parent ferricinium cation 1.697 Å) and experimental (within the range 1.69−1.70 Å) data.[29] The same holds for a similar elongation on moving from ruthenocene to ruthenicinium

(27) (a) Demadis, K.; Hartshorn, C. M.; Meyer, T. J. *Chem. Rev.* **2001**, *101*, 2655. (b) D'Alessandro, D.; Keene, F. R. *Chem. Soc. Rev.* **2006**, *35*, 424.

(28) The magnitude of the Γ parameter, $\Gamma = 1 - (\Delta\nu_{1/2}°/\Delta\nu_{1/2})$, distinguishes the class of mixed-valence system: $0 < \Gamma < 0.1$ for weakly coupled Class II system, $0.1 < \Gamma < 0.5$ for moderately coupled Class II systems, $\Gamma = 0.5$ at the transition between Class II and Class III, and $\Gamma > 0.5$ for Class III. See: Brunschwig, B. S.; Creutz, C.; Sutin, N. *Chem. Soc. Rev.* **2002**, *31*, 168.

(29) (a) Dunitz, J. D.; Orgel, L. E.; Rich, A. *Acta Crystallogr.* **1956**, *9*, 373. (b) Bats, J. V.; de Boer, J. S.; Bright, D. *Inorg. Chim. Acta* **1971**, *5*, 605. (c) Mammano, N. J.; Zalkin, A.; Landers, A.; Rheingold, A. L. *Inorg. Chem.* **1977**, *16*, 297. (d) Churchill, M. R.; Landers, A. G.; Rheingold, A. L. *Inorg. Chem.* **1981**, *20*, 849.

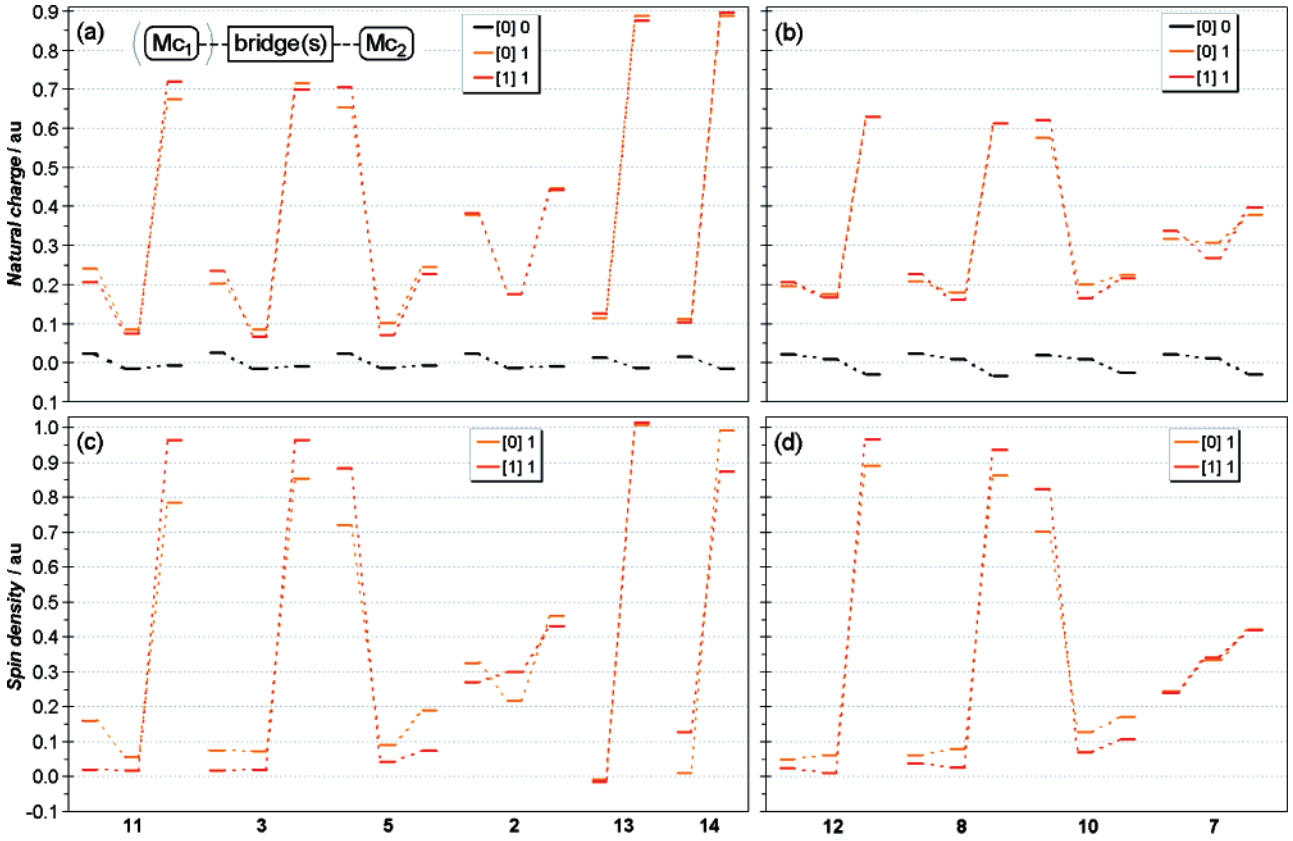

FIGURE 6. Calculated distribution of natural charge (a and b) and Mulliken spin density (c and d) in all studied compounds in their neutral form (black) and mono-oxidized forms before (orange) and after (red) structural relaxation. For every compound, Mc_1−bridge−Mc_2, the central line represents the bridge and those at the left and right sides sketch the Mc_1 and Mc_2 units, respectively. Compounds **13** and **14** are represented in the "bridge−Mc_2" form (i.e., the only metallocenyl group is denoted as Mc_2 and the left-side line represents the vinyl group).

(calculated $d_{Ru-Cp\#}$ = 1.870 and 1.910 Å, respectively). Therefore, the above distance is a suitable parameter for measuring the oxidation degree at a ferrocene unit. The variation of M−$Cp_{b\#}$ distance between the [0]0 and [1]1 states at both Mc units (ends of every line) is plotted in Figure 7a for the systems under consideration.

Two other reported geometric parameters, such as the exocyclic bond bent angle, α, and the inter-rings tilt angle at the respective midpoints, β[30] (see the Supporting Information), have proved to be useful for the characterization of geometrical distortions at ferrocene units, specially when attached to electrodeficient substituents. Nevertheless, the definition of the bent angle merits special care (see the Supporting Information) as far as different related (ill-defined) meanings can be found in the literature. High β values account for a tilting of the Fe d_{z^2}-type orbital which is involved in the σ interaction with both the a_{1g}-type MO of the Cp_b unit and the lowest unoccupied molecular orbital (LUMO) (π^*) of the fulvene-type ligand containing Cp_a and the adjacent bridge C atom. The latter interaction is said to be responsible for weakening of the exocyclic bond and so allowing bending toward iron (i.e., increasing of α).[31] We have found that α values and their increments scatter within the studied compounds being only of little significance for some general trends, while β angle variation along the oxidative sequence is very characteristic of the different behavior of every metallocene unit (Figure 7b),

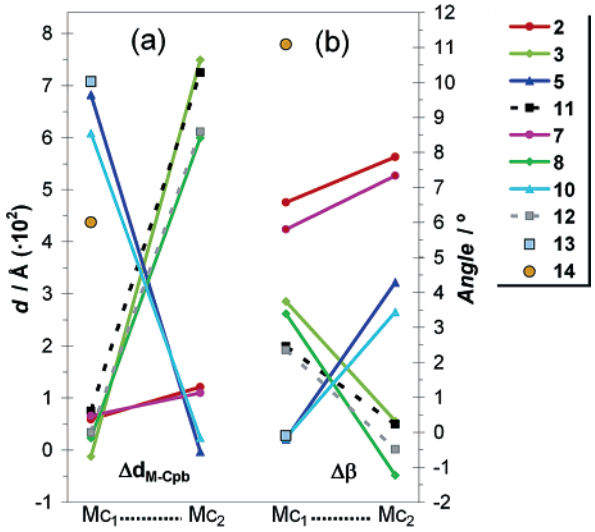

FIGURE 7. Variation of selected geometric parameters upon one-electron oxidation (from [0]0 to [1]1 states) in all studied compounds at both metallocene subunits: (a) distance between the metal atom and the Cp_b (the free Cp ring whenever possible) ring centroid; (b) inter-rings tilt angle at the respective midpoints, β.

being very sensitive to both its own oxidation degree and that at the neighbor metallocene, and with the advantage that it applies to both ferrocenes and ruthenocenes. Thus, in the simplest compounds considered herein, the ferricinium unit in $\mathbf{13}^{\bullet+}$ exhibits near zero $\Delta\beta$ value with very large Fe−$Cp_{b\#}$

(30) Gleiter, R.; Seeger, R. *Helv. Chim. Acta* **1971**, *54*, 1217.
(31) Lupan, S.; Cais, M.; Herbstein, F. H.; Kapon, M. *Angew. Chem., Int. Ed. Engl.* **1972**, *11*, 1025.

distance elongation whereas the formal ruthenocinium moiety in **14**$^{\bullet+}$ displays a middle-range distance elongation and the highest increment in tilt angle ($\Delta\beta = 11.1°$) supplemented by very high inward bending of the exocyclic bond ($\Delta\alpha = 6.9°$) that indicates strong donor−acceptor interaction of the exocyclic α position with the formal Ru(III) center resulting in the actual oxidation of the former (see above and Figure 6c).

As expected, all dyads with a ferrocene Mc_2 unit (**3**, **8**, **11**, and **12**) experience similar oxidative behavior resulting in a fully oxidized $Fc_2^{\bullet+}$ moiety bearing most of the positive charge ($\Delta q = 0.64-0.73$ au, Figure 6a and b) and virtually all the spin density (range 0.93−0.97 au, Figure 6c and d), in agreement with a large elongation of the Fe−Cp_b distance in Fc_2 (range 0.060−0.075 Å) and only residual variation of tilt angle (range −1.2 to 0.3°) and, on the contrary, nearly vanishing elongation in Mc_1 (range −0.001 to 0.008 Å) with moderate tilt angle increment (range 3.4−3.7°). Compounds **5** and **10** exhibit similar behavior as **3** and **8** upon oxidation by exchanging the roles of Mc_1 and Mc_2, both under the electronic and the geometric viewpoints, although in these cases some small but significant (more than "residual") spin density is allocated at either the formally unoxidized Rc_2 unit or the bridge. Finally, diruthenocenyl dyads **2** and **7** behave in a rather different way after one-electron removal as far as the acquired positive charge is unsymmetrically spread over both Rc moieties, originating formal $Ru^{2.5}Ru^{2.5}$ species, and also significantly over the bridge ($\Delta q = 0.19$ and 0.26 au for **2** and **7**, respectively) which therefore results formally oxidized (Figure 6a and b), which is furthermore evidenced by the distribution of spin density over all the molecule (Figures 6c and d and 9b), the low elongation of the Ru−Cp_b* distance (Figure 7a), and the unusually high increase of tilt angle (Figure 7b) at both Mc units in similar extents.

Also a well-known way for ferrocene and ruthenocene units to stabilize adjacent electron deficiencies is by shifting to a (η^5-ciclopentadienyl)M(η^6-fulvene) binding mode,[4,32] which in turn can be pointed out by an increase of the bond length alternation along the Cp ring and the exocyclic bond. This is in fact what is observed in all dicationic species derived from the molecular systems under consideration (calculated in their more stable triplet spin states for those dications having at least one ferrocene group but as the more stable singlet states for the diruthenocenyl dications) but is specially interesting for the mono-oxidized radical-cation species where relevant information can be grasped. Thus, although not parametrized, relatively enhanced bond length alternation is observed in most species displaying high β values and seems to have special relevance in diruthenocenyl radical-cations **2**$^{\bullet+}$ and **7**$^{\bullet+}$ where the positive charge and spin density are effectively delocalized over all the molecule.

Finally, the occurrence of MMCT transitions in the studied MV compounds can be rationalized in the light of frontier MO (FMO) qualitative analysis and time-dependent DFT (TDDFT) calculations. Although it is well-known that ferrocene is the stronger donor in the electron-transfer sense as stated before, it does not necessarily mean a greater perturbation of an attached π-conjugated system, since the detail of the electronic coupling between them is also critical. Indeed, it has been shown[33] that the most significant perturbation experienced by the metallocene electronic levels is not to the metal-based HOMOs but to the highest "ligand" levels. So long as the acceptor unit is sufficiently strong that its empty acceptor orbital lies below the metallocene LUMOs (cpd_{xz} and cpd_{yz}, keeping the orbital designations for the isolated parent ferrocene having D_{5h} symmetry), the resulting LUMO of the dyad is centered on the acceptor moiety with some delocalization onto the π-bridge. In these cases, both crystallographic and NMR data for neutral dyads[13] indicate that a zwitterionic resonance form involving a η^6-coordination gains in importance, this resulting in a reduction in the bond-length alternation (BLA) within the insaturated bridge (Figure 8). There is electrochemical evidence[27] that, despite having a lower energy HOMO than ferrocene, ruthenocene is the stronger donor in conjugated systems because of the more extensive d-orbitals at ruthenium and its consequent tendency to shift toward η^6-fulvene coordination.

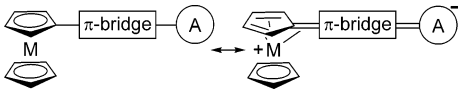

FIGURE 8. Resonance structures for π-conjugated metallocene-acceptor dyads.

A blow-up of the FMO diagram for radical-cations **11**$^{\bullet+}$, **3**$^{\bullet+}$, **5**$^{\bullet+}$, and **2**$^{\bullet+}$ is depicted in Figure 9 (see also the Supporting Information for expanded MO diagrams), and Table 3 contains results of TDDFT calculations for the lowest-energy transitions together with their assignment. Although the absolute values of the theoretically determined transition energies differ appreciably from the experimental data (Table 1), they provide information regarding the energetic sequence of the electronic transitions. The main effect observed in the MO diagram is the existence of a low-lying β-LUMO consisting of an antibonding combination of the bridge HOMO-1 (the one-node dienic MO) with the d_{x2-y2}-type MO[34] of both metallocenes, having larger coefficients at the most positively charged (most oxidized) metallocene. All ferricinium-containing monooxidized species **11**$^{\bullet+}$, **3**$^{\bullet+}$, and **5**$^{\bullet+}$ have high calculated electric dipole moments (10.18, 11.09, and 10.78 D, respectively), and their lowest energy band in the near-IR corresponds to an optical transition from the β-HOMO, mainly centered on the other "neutral" metallocene ($d_{x^2-y^2}$-type), to the above-mentioned β-LUMO. Therefore, it is assignable to an M(II)→M(III) MMCT transition which is X-polarized (i.e., in the bridge direction) and hence electric-dipole (ED) allowed. The low intensity of the MMCT band in **5**$^{\bullet+}$ could be explained by the lower X-polarization of this electronic transition as a consequence of the higher mixing between Mc units in both β-HOMO and β-LUMO (Figure 9). This could be explained by the higher tendency of the formally unoxidized ruthenocene unit to delocalize the positive charge according to the resonance structure shown in Figure 8.

On the contrary, in the case of **2**$^{\bullet+}$ both metal centers are very weakly coupled to each other because of the oxidation of the bridge so that the unpaired electron is delocalized over all the molecule, as indicated by the very low calculated dipole moment (1.78 D) and the high spreading of the key FMO. As a result, there is little net movement of the centers of charge associated with transitions corresponding to near-IR bands where only a very weak signal (not collected in Table 1) around 1096 nm ($\epsilon \approx 0.001$ $M^{-1}cm^{-1}$), ascribable to a Ru_1-to-bridge d_{z^2}-π* MLCT transition of vanishing ED intensity, could be hardly distinguished above noise.

(32) Hill, E. A.; Richards, S. H. *J. Am. Chem. Soc.* **1961**, *83*, 3840.
(33) Barlow, S.; Marder, S. R. *Chem. Commun.* **2000**, 1555.

(34) The coordinate system is oriented such that the *x* axis is along the azadiene bridge and the *z* axis is perpendicular to every Cp_a plane.

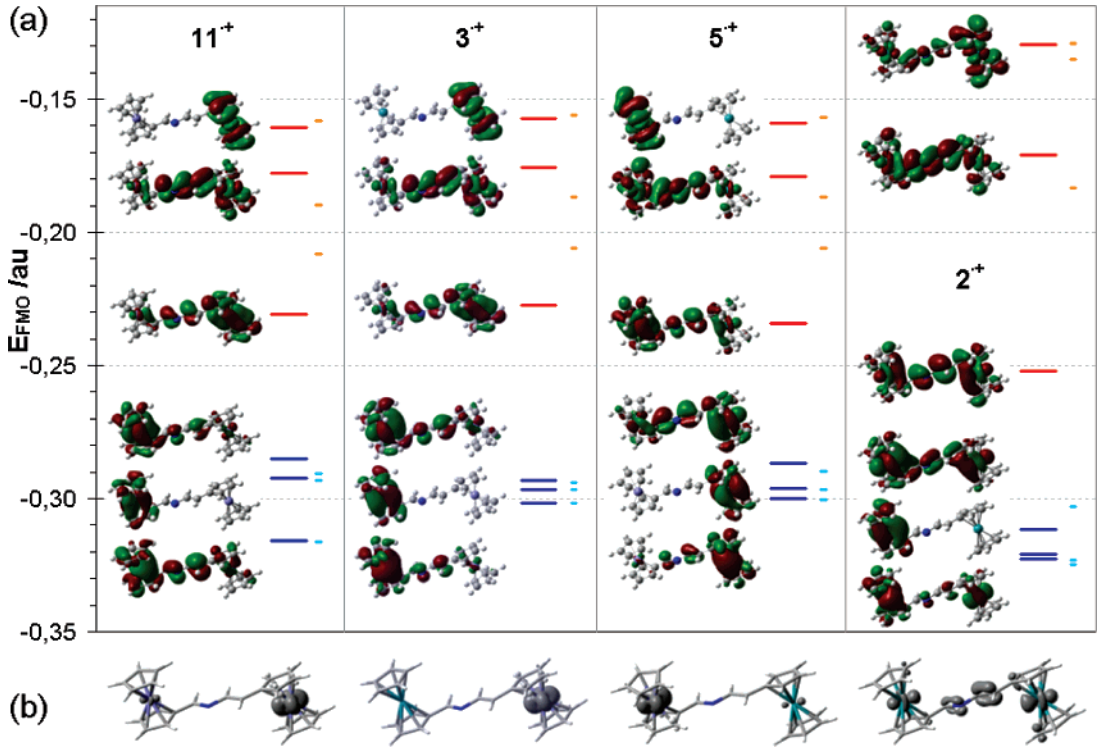

FIGURE 9. (a) Calculated (B3LYP/6-31G*/Lanl2DZ-ECP) detailed scheme for the β-spin MO (0.02 isovalue) and (b) Mulliken spin density distribution (0.005 isovalue) for optimized geometries of radical cations **11**•+, **3**•+, **5**•+, and **2**•+. Only three HOMOs (blue) and three LUMOs (red) are sketched. Short (cyan and orange) lines on right represent the energy of the FMO in the α-series.

TABLE 3. TDDFT Calculated Lowest-Energy Electronic Transitions

	λ_{max}[a]	f[b]		assignment
11•+	1844	0.025	MMCT	β-HOMO→LUMO
	2	0.068	MLCT	α-HOMO→LUMO
	907.0	0.034	MLCT	β-HOMO→LUMO+1
	637.2	0.061	MLCT	α-HOMO-2→LUMO
	616.0	0.051	*d*→π*	α-HOMO→LUMO+3
	525.0			
3•+	1156	0.036	MMCT	β-HOMO→LUMO
	6	0.155	MLCT	α-HOMO→LUMO
	692.0	0.027	MLCT	β-HOMO-3→LUMO
	682.7	0.030	MLCT	α-HOMO-2→LUMO
	626.1	0.177	*d*→π*	β-HOMO→LUMO+1
	514.4			
5•+	1732	0.066	MMCT	β-HOMO→LUMO
	0	0.155	*d*→π*	α-HOMO→LUMO
	764.8	0.010	MLCT	α-HOMO→LUMO+1
	569.1	0.241	MLCT	β-HOMO→LUMO+1
	560.1			
2•+	1409	0.014	*d*→π*	β-HOMO-1→LUMO
	3	0.133	MLCT	β-HOMO-3→LUMO
	1096.	0.061	LMCT	β-HOMO-8→LUMO
	0	0.756	π→π*	α-HOMO→LUMO
	581.6			
	504.7			

[a] Unscaled (nm). [b] Oscillator strength (au).

Metal-Ion Sensing Properties. One of the most interesting attributes of dyads **2**, **3**, and **5** and metallocenophanes **7**, **8**, and **10** is the presence of differentiated redox-active metallocenes close to the cation-binding nitrogen atom. Therefore, the metal recognition properties of these aza-substituted metallocenes toward Li^+, Na^+, K^+, Ca^{2+}, Mg^{2+}, Zn^{2+}, Cd^{2+}, Hg^{2+}, and Ni^{2+} metal ions (as their perchlorate salts) were evaluated by UV/vis spectroscopy, because previous studies on ferrocene ligands have shown that the characteristic lowest energy metal-to-ligand (MLCT) transition is perturbed by complexation.[35] Titration experiments for dichloromethane solutions of ligand ($c = 10^{-4}$ M) and the corresponding ions were performed and analyzed quantitatively.[36]

Whereas no perturbation of the absorption spectra of the bimetallocene dyads **2**, **3**, and **5** were observed upon addition of Li^+, Na^+, K^+, and Ca^{2+}, even in a large excess, a significant red-shift of both the high- (HE) and low-energy (LE) absorption bands were observed upon addition of Mg^{2+} ions. Thus, the addition of increasing amounts of $Mg(ClO_4)_2$ to a solution of **2** in CH_2Cl_2 caused a red-shift of the HE band of 49 nm along with a progressive appearance of a new band located at $\lambda =$ 457 nm as well as the complete disappearance of the initial

(35) Carr, J. D.; Coles, S. J.; Asan, M. B.; Hurthouse, M. B.; Malik, K. M. A.; Tucker, J. H. R. *J. Chem. Soc., Dalton Trans.* **1999**, 57.

(36) Specfit/32 Global Analysis System, 1999−2004 Spectrum Software Associates. SpecSoft@compuserve.com. The Specfit program was acquired from Bio-Logic, SA (www.bio-logic.info) in January 2005.

(37) Frisch, M. J.; Trucks, G. W.; Schlegel, H. B.; Scuseria, G. E.; Robb, M. A.; Cheeseman, J. R.; Montgomery, J. A., Jr.; Vreven, T.; Kudin, K. N.; Burant, J. C.; Millam, J. M.; Iyengar, S. S.; Tomasi, J.; Barone, V.; Mennucci, B.; Cossi, M.; Scalmani, G.; Rega, N.; Petersson, G. A.; Nakatsuji, H.; Hada, M.; Ehara, M.; Toyota, K.; Fukuda, R.; Hasegawa, J.; Ishida, M.; Nakajima, T.; Honda, Y.; Kitao, O.; Nakai, H.; Klene, M.; Li, X.; Knox, J. E.; Hratchian, H. P.; Cross, J. B.; Bakken, V.; Adamo, C.; Jaramillo, J.; Gomperts, R.; Stratmann, R. E.; Yazyev, O.; Austin, A. J.; Cammi, R.; Pomelli, C.; Ochterski, J. W.; Ayala, P. Y.; Morokuma, K.; Voth, G. A.; Salvador, P.; Dannenberg, J. J.; Zakrzewski, V. G.; Dapprich, S.; Daniels, A. D.; Strain, M. C.; Farkas, O.; Malick, D. K.; Rabuck, A. D.; Raghavachari, K.; Foresman, J. B.; Ortiz, J. V.; Cui, Q.; Baboul, A. G.; Clifford, S.; Cioslowski, J.; Stefanov, B. B.; Liu, G.; Liashenko, A.; Piskorz, P.; Komaromi, I.; Martin, R. L.; Fox, D. J.; Keith, T.; Al-Laham, M. A.; Peng, C. Y.; Nanayakkara, A.; Challacombe, M.; Gill, P. M. W.; Johnson, B.; Chen, W.; Wong, M. W.; Gonzalez, C.; Pople, J. A. *Gaussian 03*, Revision B.03; Gaussian, Inc.: Wallingford, CT, 2004.

(38) Bartolotti, L. J.; Fluchick, K. In *Reviews in Computational Chemistry*; Lipkowitz, K. B., Boyd, B. D., Eds.; VCH: NewYork, 1996; Vol. 7, p 187.

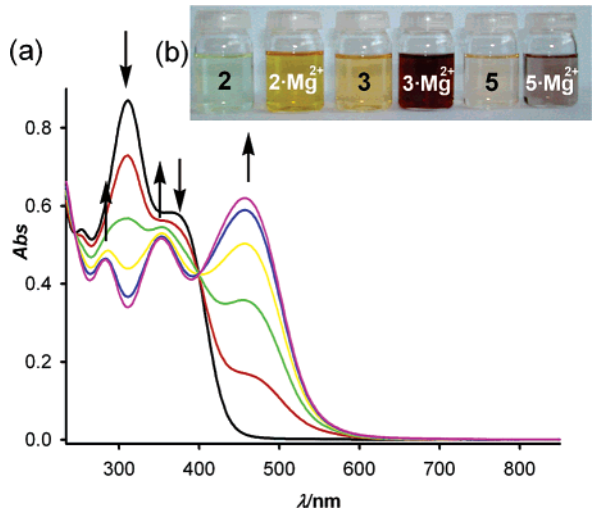

FIGURE 10. (a) Changes in the absorption spectra of compound **2** (0.1 mM) in CH_2Cl_2 upon addition from 0 (black) to 0.5 (purple) equiv of Mg^{2+} ion. Arrows indicate absorptions that increase or decrease during the experiment. (b) Changes in the color of the ligands **2**, **3**, and **5** upon addition of Mg^{2+}ion.

band at 365 nm. A well-defined isosbestic point at 399 nm indicates that a neat interconversion between the uncomplexed and complexed species occurs (Figure 10). The new LE band is red-shifted by 92 nm and is responsible for the change of color, which can be used for a "naked-eye" detection of Mg^{2+} ions in the presence of Ca^{2+} ions. The resulting titration fitted to a 2:1 (ligand/metal ion) binding model and ln $K_{as} = 7.9 \pm 0.52$.

For dyads **3** and **5**, the HE and LE bands were also red-shifted by 36−38 nm and 83−85 nm, respectively, upon addition of Mg^{2+} ions, and well-defined isosbestic points, at $\lambda = 349$ and 359 nm, respectively, were also observed. The titrations fitted to 2:1 (ligand/metal ion) binding models, with ln $K_{as} = 8.2 \pm 0.54$ for **3**·Mg^{2+} and ln $K_{as} = 7.8 \pm 0.41$ for **5**·Mg^{2+}. Surprisingly, the optical-sensing behavior of these ferrocene−ruthenocene dyads toward the divalent Zn^{2+}, Cd^{2+}, Hg^{2+}, and Ni^{2+} metal ions were found to be identical to those found with Mg^{2+} metal ions (Table 4).

From a ^{1}H NMR spectroscopy analysis, it was possible to obtain additional information about the coordination of the Mg^{2+} by ligand **3** in $CDCl_3$. The spectrum of the free ligand shows the typical pattern of signals corresponding to the monosubstituted ferrocene and ruthenocene as well as those corresponding to the 2-aza-1,3-butadiene bridge.

While the pattern due to the monosubstituted ferrocene unit does not change upon addition of 0.5 equiv of Mg^{2+} metal ion, the following significant changes are evidenced in the other regions of the spectrum: (1) the iminic proton (7.96 ppm) moves to downfield (9.11 ppm); (2) the two well-separated doublets ($\Delta\delta = 0.96$ ppm) due to the ethylenic protons of the bridge appear now almost overlapped ($\Delta\delta = 0.11$ ppm ppm), one is downfield shifted from 6.60 to 6.68 ppm and the other is upfield shifted from 6.96 to 6.79 ppm, respectively; (3) the two signals due to the monosubstituted Cp ring of the ruthenocene unit are cleanly downfield shifted by 0.13 and 0.27 ppm, respectively. From the magnitude of these observed shifts, it can be surmised that the coordination, in this case, exerts a more powerful deshielding effect on the ruthenocene and the 2-aza-1,3-butadiene bridge units than on the ferrocene units (Figure 11).

As far as double-bridged compounds are concerned, no changes were observed in the UV/vis spectra of all bimetallocenophanes **7**, **8**, and **10** upon addition of one equivalent of Li^+, Na^+, K^+, and Ca^{2+} metal ions. However, it is important to underline that, from the spectrophotometric behavior of these derivatives upon addition of Mg^{2+}, Zn^{2+}, Cd^{2+}, Hg^{2+}, and Ni^{2+} metal ions, it is clear that the binding events are strongly affected by the relative position and nature of the metallocenes subunits in the metallocenophane framework. Addition of the above-mentioned set of divalent metal cations to the diaza[4.4]-ruthenocenophane **7** induced a red-shift (73 nm) of the LE band from 336 to 409 nm, whereas the Hg^{2+} ion promoted a slightly slower red-shift by 65 nm, and in all cases a clear isosbestic point at 318 nm was observed during the titrations experiments. The heterobimetallocenophane **8** displays a similar optical-sensing behavior with a higher red-shift of the LE band with concomitant color change. Thus, the addition of increasing amounts of Cd^{2+} ion to a solution of **8** in CH_2Cl_2 caused a slight red-shift of the HE band of 35 nm along with a progressive appearance of a new band located at $\lambda = 638$ nm as well as the complete disappearance of the initial band at 492 nm. A well-defined isosbestic point at $\lambda = 327$ nm indicates that a neat interconversion between the uncomplexed and complexed species occurs (Figure 12).

The new LE band is red-shifted by 146 nm and is responsible for the change of color, with the resulting titration fitted to a 1:1 (ligand/metal ion) binding model and ln $K_{as} = 5.9 \pm 0.31$. Divalent Zn^{2+}, Cd^{2+}, Hg^{2+}, and Ni^{2+} metal ions promoted a higher red-shift from $\lambda = 492$ to 677 nm. The new LE band is red-shifted by 185 nm and is responsible for the change of color, with the resulting titrations fitted to a 1:1 (ligand/metal ion) binding mode. In all cases, the appearance of an isosbestic point at $\lambda = 330$ nm during the spectral titrations suggests the formation of well-defined complexes between **8** and the tested cations that should be responsible for the new and red-shifted absorption band. Surprisingly, the absorption spectrum of the regioisomer **10** remains unaltered upon addition of the above-mentioned divalents cations. Also, addition of cations (not shown) beyond the point of equivalence for each complex did not cause a significant change in the absorption spectra. Titration analysis data gave the stability constants displayed in Table 4 and confirmed the formation in solution of the reported ligand: metal stoichiometries.

For the reported constants to be taken with confidence, we have proved the reversibility of the complexation process by carrying out the following experimental test: 0.5 equiv of $Mg(ClO_4)_2$ was added to a solution of **3** in CH_2Cl_2 to obtain the complexed **3**$_2$·Mg^{2+} species, whose DPV voltammogram and UV/vis spectrum were recorded. The CH_2Cl_2 solution of the complex was washed several times with water until the color of the solution changed from deep red to pale yellow. The organic layer was dried and the optical spectrum, DPV voltammogram, and ^{1}H NMR spectrum were recorded and they were found to be the same as that of the free-receptor **3**. Afterward, 0.5 equiv of $Mg(ClO_4)_2$ was added to this solution and the initial UV/vis spectrum, DPV voltammogram, and ^{1}H NMR spectrum of the complex **3**$_2$·Mg^{2+} were fully recovered together with the deep red color. This experiment was carried out over several cycles, and the optical spectrum was recorded after each step and was fully recovered on completion of the step, thus demonstrating the high degree of reversibility of the complexation/decomplexation process. Similar studies were carried out

TABLE 4. Relevant Physicochemical Data of the Ligand/Metal Complexes Formed

comp		Cd^{2+}	Zn^{2+}	Hg^{2+}	Ni^{2+}	Pb^{2+}
2	λ^a	352 (6.14), 457 (7.43)	352 (6.24), 457 (8.31)	336 (7.35), 449 (5.03)	352 (6.27), 457 (7.69)	352 (6.57), 457 (7.04)
	$\Delta\lambda^b$	92	92	84	92	92
	log $K_{as}{}^c$	8.1 ± 0.33	7.8 ± 0.30	6.5 ± 0.31	8.2 ± 0.29	7.9 ± 0.31
	L/M^d	2/1	2/1	2/1	2/1	2/1
3	λ^a	358 (12.80), 424 (9.41), 533 (4.91)	358 (12.97), 424 (9.57), 533 (4.97)	358 (12.79), 424 (8.16), 533 (4.27)	358 (12.83), 424 (9.44), 533 (4.91)	358 (12.66), 424 (8.80), 533 (4.6)
	$\Delta\lambda^b$	85	85	85	85	85
	log $K_{as}{}^c$	8.0 ± 0.40	8.1 ± 0.30	7.9 ± 0.35	8.2 ± 0.37	8.1 ± 0.31
	L/M^d	2/1	2/1	2/1	2/1	2/1
5	λ^a	369 (8.11), 445 (sh), 547 (3.74)	369 (8.26), 445 (sh), 547 (3.89)	369 (7.98), 445 (sh), 547 (3.69)	369 (8.17), 445 (sh), 547 (3.82)	369 (7.99), 445 (sh), 547 (3.31)
	$\Delta\lambda^b$	83	83	83	83	83
	log $K_{as}{}^c$	7.9 ± 0.35	8.1 ± 0.30	7.5 ± 0.33	8.0 ± 0.33	7.7 ± 0.29
	L/M^d	2/1	2/1	2/1	2/1	2/1
7	λ^a	342 (14.85), 409 (8.99)	335 (16.50), 409 (9.27)	327 (17.89), 401 (7.76)	340 (15.82), 409 (8.70)	293 (15.97), 332 (13.83), 409 (4.92)
	$\Delta\lambda^b$	73	73	65	73	73
	log $K_{as}{}^c$	6.5 ± 0.35	6.4 ± 0.34	6.5 ± 0.41	6.4 ± 0.33	5.9 ± 0.31
	L/M^d	**1/1**	**1/1**	**1/1**	**1/1**	**1/1**
8	λ^a	356 (22.63), 437 (4.18), 485 (sh), 677 (1.15)	355 (22.91), 440 (4.18), 485 (sh), 675 (1.17)	356 (22.60), 438 (4.19), 485 (sh), 677 (1.16)	356 (22.90), 440 (4.29), 485 (sh), 674 (1.16)	348 (11.78), 434 (3.04), 638 (0.08)
	$\Delta\lambda^b$	185	183	185	182	146
	log $K_{as}{}^c$	6.5 ± 0.35	6.4 ± 0.34	6.5 ± 0.41	6.4 ± 0.33	5.9 ± 0.31
	L/M^d	1/1	1/1	1/1	1/1	1/1

^{a} λ_{max}, in nm; ϵ, in dm^3 mol^{-1} cm^{-1}. ^{b} Red-shift of the LE band upon metal complexation ($\Delta\lambda = \lambda_{complexed} - \lambda_{free}$). ^{c} Association constant determined by Specfit/32 Global Analysis System. ^{d} Stoichiometry of the complex formed (ligand/metal).

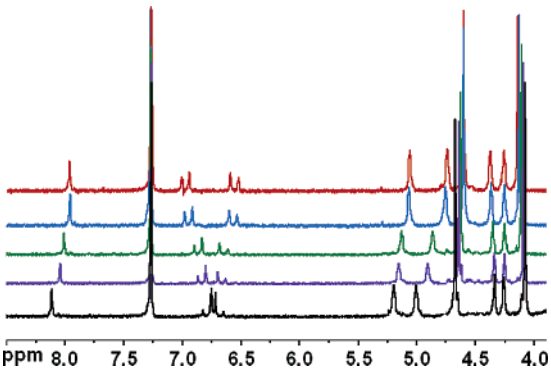

FIGURE 11. Evolution of the ^{1}H NMR spectra of **3** (red) upon addition of increasing amounts of Mg^{2+} until 0.5 equiv was added (black).

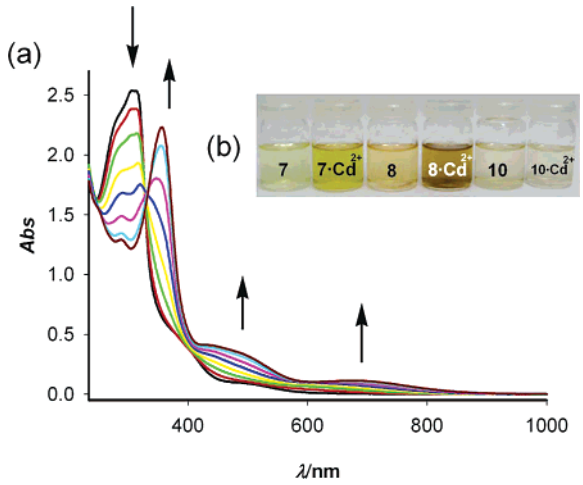

FIGURE 12. (a) Changes in the absorption spectra of compound **8** (0.1 mM) in CH_2Cl_2 upon addition from 0 (black) to 1 (purple) equiv of Cd^{2+} ion. Arrows indicate absorptions that increase or decrease during the experiment. (b) Changes in the color of the ligands **7**, **8**, and **10** upon addition of Cd^{2+} ion.

using the receptors **2**, **5**, and **8** and Cd^{2+}, Zn^{2+}, and Hg^{2+} cations, which confirm the reversibility of this process between each metallocene and the cationic metal species. Moreover, stepwise addition of a solution of receptor **2** in CH_2Cl_2 to a solution of the complex $\mathbf{2}_2{\cdot}Mg^{2+}$ in the same solvent induced an increase of the absorption band in the optical spectrum of the receptor in proportion to the amount added. This fact can also be taken with high confidence as evidence for reversibility.

To study the selectivity of these complexation processes, competitive binding assays between all the metal cations studied and the receptors have been carried out. Thus, addition of 0.5 equiv of an equimolecular mixture of Cd^{2+}, Zn^{2+}, Hg^{2+}, Ni^{2+}, and Pb^{2+} cations in CH_2Cl_2 to 1 equiv of the receptors 2, 3, 5, 7, and 8 in the same solvent gave identical optical response, position, and intensity as the low-energy absorption band to those observed upon addition of 0.5 equiv of each one of the tested metal cations. These results clearly show that this kind of receptor is not selective toward the metal cations tested. One of the most interesting aspects is the discrimination between Mg^{2+} and Ca^{2+} cations.

Conclusion

In summary, new structural motifs based on "open" and "closed" ferrocene−ruthenocene dyads linked by azabridges, which could serve as important benchmarks for the investigation of intramolecular electron transfer and for metal recognition processes, are reported. Our synthetic methodology, which allows the preparation of a wide variety of ferrocene−ruthenocene either acyclic or metallocenophane-based cyclic architectures, is based on the temporal condensation of the readily available diethyl aminomethylphosphonate with the appropriate formyl metallocene and subsequent reaction of the resulting phosphonate with the same or different formyl metallocene. The ferrocene−ruthenocene dyad **3** and the new

structural motif diaza[4.4]ruthenocenoferrocenophane **8** comprise a remarkable multifunctional molecular system. In both compounds, the ruthenocene moiety displays a rather unusual quasireversible ($\Delta Ep = 0.11$ V) oxidation process, and the presence of low-energy bands in the NIR region in the monooxidized forms indicates the existence of optical-induced ICTs between the iron and ruthenium redox centers. These systems have also shown to be efficient optical and robust sensors for Mg^{2+}, Zn^{2+}, Cd^{2+}, Hg^{2+}, and Ni^{2+} cations. The new LE band is responsible for a change of color, which can be used for naked-eye detection of Mg^{2+} cations in the presence of Ca^{2+} cations. The experimental data and conclusions about the electronic properties are supported by DFT computations.

Experimental Section

General Procedure for the Preparation of N-Substituted Diethyl Aminomethylphosphonates 1 and 6. To a mixture of diethyl aminomethylphosphonate (0.157 g, 0.93 mmol) and anhydrous Na_2SO_4 (10 g) in dry CH_2Cl_2 (30 mL), the appropriate amount of the formyl metallocene was added dropwise. The resulting solution was stirred at room temperature for 2 h and then was filtered. From the filtrate, the solvent was removed under vacuum to give the corresponding aminomethylphosphonate in almost quantitative yield, as colored oils which were used, without further purification, in the next step.

Diethyl *N*-Ruthenocenylmethylidenaminomethylphosphonate, (1). ^{1}H NMR (400 MHz, $CDCl_3$): δ 1.35 (t, 6H, $^4J_{H,P} = 7.2$ Hz), 3.88 (d, 2H, $^2J_{H,P} = 17.5$ Hz), 4.13−4.20 (m, 4H), 4.61 (s, 5H,), 4.70 (st, 2H), 5.00 (st, 2H), 8.04 (d, 1H, $^4J_{H,P} = 4.8$ Hz). ^{13}C NMR (100 MHz, $CDCl_3$): δ16.4 (d, $^3J_{P,C} = 5.6$ Hz), 57.1 (d, $^1J_{P,C} = 150.9$ Hz) 62.4 (d, $^2J_{P,C} = 6.6$ Hz), 69.9 (5CH), 71.2 (2CH), 72.1 (2CH), 85.1 (d, $^4J_{P,C} = 9.0$ Hz, q), 164.4 (d, $^3J_{P,C} = 21.5$ Hz); ^{31}P NMR (162.29 MHz, $CDCl_3$): δ 22.3. MS (70 eV, EI): *m*/*z* (relative intensity): 409 (17, M^+), 245 (40), 167 (53), 149 (56), 125 (73), 111 (84), 99 (98), 81 (100), 71 (57), 57 (81).

Diethyl 1,1′-Ruthenocenediyl-bis-(methylidenaminomethylphosphonate), (6). ^{1}H NMR (400 MHz, $CDCl_3$): δ 1.36 (t, 12H, $^4J_{H,P} = 7.1$ Hz), 3.88 (d, 4H, $^2J_{H,P} = 17.0$ Hz), 4.10−4.24 (m, 8H), 4.77 (t, 4H), 5.01 (t, 4H), 8.03 (d, 2H, $^4J_{H,P} = 4.8$ Hz). ^{13}C NMR (100 MHz, $CDCl_3$): δ 16.9 (d, $^3J_{P,C} = 5.6$ Hz), 57.5 (d, $^1J_{P,C} = 151.0$ Hz), 62.4 (d, $^2J_{P,C} = 6.6$ Hz), 71.9 (2CH), 73.9 (2CH), 85.5 (d, $^4J_{P,C} = 9.1$ Hz, q), 164.5 (d, $^3J_{P,C} = 21.5$ Hz, CH═N). ^{31}P NMR (162.29 MHz, $CDCl_3$): δ 22.8. MS (FAB^+): *m*/*z* (relative intensity): 588 (100, M^++1).

General Procedure for the Preparation of 1,4-Bismetallocenyl-2-aza-1,3-butadienes. To a solution of the appropriate diethyl aminomethylphosphonate (0.93 mmol) in dry THF (20 mL), at −78 °C and under nitrogen atmosphere, the appropriate amount of *n*-butyllithium 1.6 M in hexane (0.59 mL) was dropped. Then, a solution of the appropriate amount of the formyl metallocene in dry THF (10 mL) was added dropwise and the mixture was stirred for 1.5 h. The reaction mixture was allowed to reach the room temperature and then it was heated under reflux temperature overnight. After the solution was cooled to room temperature, the solvent was evaporated under reduced pressure and the resulting solid was slurried with diethyl ether (25 mL) to give a crude product which was recrystallized from dichloromethane/diethyl ether (1/10).

1,4-Bis(ruthenocenyl)-2-aza-1,3-butadiene, (2). 80%; mp: >300 °C. ^{1}H NMR (400 MHz, $CDCl_3$): δ 4.52 (s, 5H), 4.58−4.59 (m, 7H), 4.72 (st, 2H), 4.78 (st, 2H), 5.03 (st, 2H), 6.43 (d, 1H, $J =$ 13.3 Hz), 6.91 (d, 1H, $J =$ 13.3 Hz,), 7.92 (s, 1H); ^{13}C NMR (100 MHz, $CDCl_3$): δ 69.0 (2CH), 70.4 (2CH), 70.6 (2CH), 71.1 (5CH), 71.3 (5CH), 72.3 (2CH), 85.2 (q), 85.8 (q), 125.3 (CH), 139.8 (CH), 158.3 (CH). MS (70 eV, EI): *m*/*z* (relative intensity): 514 (100, M^+), 256 (31), 245 (36), 232 (30), 167 (67). Anal. calcd for $C_{23}H_{21}NRu_2$: C, 53.79; H, 4.12; N, 2.73. Found: C, 53.55; H, 4.26; N, 2.46.

4-Ferrocenyl-1-ruthenocenyl-2-aza-1,3-butadiene, (3). 85%; mp: >300 °C. ^{1}H NMR (400 MHz, $CDCl_3$): δ 4.13 (s, 5H), 4.25 (st, 2H), 4.37 (st, 2H), 4.60 (s, 5H), 4.73 (st, 2H), 5.06 (st, 2H), 6.60 (d, 1H, $J =$ 13.2 Hz), 6.96 (d, 1H, $J =$ 13.2 Hz), 7.96 ppm (s, 1H). ^{13}C NMR (100 MHz, $CDCl_3$): δ 66.7 (2CH), 68.8 (2CH), 69.2 (5CH), 70.4 (2CH), 71.3 (5CH), 72.3 (2CH), 81.9 (q), 85.3 (q), 126.4 (CH), 139.9 (CH), 158.1 (CH). MS (70 eV, EI): *m*/*z* (relative intensity): 469 (100, M^+), 404 (72), 121 (60). Anal. calcd for $C_{23}H_{21}FeNRu$: C, 58.99; H, 4.52; N, 2.99. Found: C, 59.25; H, 4.40; N, 2.78.

1-Ferrocenyl-4-ruthenocenyl-2-aza-1,3-butadiene, (5). 78%; mp: >300 °C. ^{1}H NMR (400 MHz): δ 4.21 (s, 5H), 4.44 (st, 2H), 4.54 (s, 5H), 4.60 (st, 2H), 4.69 (st, 2H), 4.81 (st, 2H), 6.48 (d, 1H, $J =$ 13.3 Hz), 6.99 (d, 1H, $J =$ 13.3 Hz), 8.07 (s, 1H). ^{13}C NMR (100 MHz, $CDCl_3$): δ 68.6 (2CH), 69.1 (2CH), 69.3 (5CH), 70.6 (2CH), 71.0 (2CH), 71.1 (5CH), 80.7 (q), 86.0 (q), 125.3 (CH), 140.2 (CH), 160.0 (CH). MS (70 eV, EI): *m*/*z* (relative intensity): 469 (100, M^+), 404 (36), 375 (30), 121 (70). Anal. calcd for $C_{23}H_{21}FeNRu$: C, 58.99; H, 4.52; N, 2.99. Found: C, 58.71; H, 4.26; N, 3.20.

General Procedure for the Preparation of 2,17-Diaza-[4,4]-metallocenophanes. To a solution of the adequate N-substituted diethyl aminomethylphosphonate (**1** or **6**) (1.65 mmol) in dry THF (15 mL), at −78 °C and under nitrogen atmosphere, *n*-BuLi 1.6 M in hexane (1.10 mL) was added. To this stirred solution, a solution of the appropriate 1,1′-diformylmetallocene (0.83 mmol) in dry THF (10 mL) was slowly added and the mixture was stirred for 1.5 h. Then, the reaction mixture was allowed to reach the room temperature (30 min) and then it was heated under reflux temperature overnight. After the solution was cooled at 0 °C for 30 min, a precipitate was formed which was filtered, was washed with diethyl ether (2 × 10 mL), and was dried to give the corresponding metallocenophane, which was crystallized from THF.

2,17-Diaza-[4,4]ruthenocenophane, (7). 40%; mp: >300 °C. ^{1}H NMR (400 MHz, $CDCl_3$): δ 4.48 (st, 4H), 4.63 (st, 4H), 5.05 (st, 4H), 5.46 (st, 4H), 6.68 (d, 2H, $J =$ 13.0 Hz), 7.04 (d, 2H, $J =$ 13.0 Hz), 8.37 (s, 2H). ^{13}C NMR (100 MHz, $CDCl_3$): δ 70.4 (2CH), 70,6 (2CH), 72.5 (2CH), 72.6 (2CH), 85.4 (q), 86.0 (q), 125.4 (CH), 140.3 (CH), 159.0 (CH). MS (FAB^+): *m*/*z* (relative intensity): 565 (8, $M^+ + 1$). Anal. calcd for $C_{23}H_{22}N_2Ru_2$: C, 55.31; H, 3.93; N, 4.96. Found: C, 55.49; H, 3.72; N, 4.76.

2,17-Diaza[4.4]ruthenocenoferrocenophane, (8). 32%; mp: >300 °C. ^{1}H NMR (400 MHz, $CDCl_3$): δ 4.12 (st, 4H), 4.69 (st, 4H), 4.73 (st, 4H), 5.41 (st, 4H), 6.70 (d, 2H, $J =$ 13.0 Hz), 7.03 (d, 2H, $J =$ 13 Hz), 8.18 (s, 2H). ^{13}C NMR (100 MHz, $CDCl_3$): δ 68.0 (2CH), 68.7 (2CH), 72.1 (2CH), 72.8 (2CH), 85.1 (q), 84.6 (q), 87.7 (q), 128.6 (CH), 141.1 (CH), 158.8 (CH). MS (FAB^+): *m*/*z* (relative intensity): 520 (7, $M^+ + 1$). Anal. calcd for $C_{26}H_{22}FeN_2Ru$: C, 60.13; H, 4.27; N, 5.39. Found: C, 60.36; H, 3.98; N, 5.56.

2,17-Diaza[4.4]ferrocenoruthenocenophane, (10). 25%; mp: >300 °C. ^{1}H NMR (400 MHz, $CDCl_3$): δ 4.31 (st, 4H), 4.49 (t, 4H), 5.07 (st, 4H), 5.18 (st, 4H), 6.46 (d, 2H, $J =$ 13.0 Hz), 6.93 (d, 2H, $J =$ 13.0 Hz), 8.38 (s, 2H). ^{13}C NMR (100 MHz, $CDCl_3$): δ 68.7 (2CH), 69.3 (2CH), 69.4 (2CH), 70.6 (2CH), 80.5 (q), 86.2 (q), 125.2 (CH), 140.2 (CH), 159.8 (CH). MS (FAB^+): *m*/*z* (relative intensity): 520 (5, $M^+ + 1$). Anal. calcd for $C_{26}H_{22}FeN_2Ru$: C, 60.13; H, 4.27; N, 5.39. Found: C, 60.39; H, 4.36; N, 5.19.

Acknowledgment. We gratefully acknowledge a grant from MEC-Spain CTQ2004-02201 and from Fundación Séneca (CARM) 02970/PI/05. A.C. also thanks the Ministerio de Educación y Ciencia for a predoctoral grant.

Supporting Information Available: NMR spectra. Electrochemical data. Evolution of the UV−vis−NIR spectra during the course of the oxidation processes. Evolution of the absorption spectra upon addition of cation guests. Calculated structures, energies, and Cartesian coordinates. This material is available free of charge via the Internet at the http://pubs.acs.org.

JO0618932